JBIC Journal of Biological Inorganic Chemistry (2024) 29:353–373
https://doi.org/10.1007/s00775-024-02050-4

ORIGINAL PAPER

Biosynthesized silver nanoparticles prevent bacterial infection in chicken egg model and mitigate biofilm formation on medical catheters

Lipi Pradhan[1] · Prince Sah[1] · Malay Nayak[1] · Anjali Upadhyay[1] · Pragya Pragya[1] · Shikha Tripathi[2] · Gurmeet Singh[1] · B. Mounika[1] · Pradip Paik[1] · Sudip Mukherjee[1]

Received: 13 November 2023 / Accepted: 20 March 2024 / Published online: 14 May 2024

Abstract

Investigating the application of innovative antimicrobial surface coatings on medical devices is an important field of research. Many of these coatings have significant drawbacks, including biocompatibility, coating stability and the inability to effectively combat multiple drug-resistant bacteria. In this research, we developed an antibiofilm surface coating for medical catheters using biosynthesized silver nanoparticles (b-Cs-AgNPs) developed using leaves extract of *Calliandra surinamensis*. Various characterization techniques were employed to thoroughly characterize the synthesized b-Cs-AgNPs and c-AgNPs. b-Cs-AgNPs were compatible with human normal kidney cells and chicken embryos. It did not trigger any skin inflammatory response in in vivo rat model. b-Cs-AgNPs demonstrated potent zone of inhibition of 19.09 mm when subjected to the disc diffusion method in *E. coli* confirming strong antibacterial property. Different anti-bacterial assays including liquid growth curve, colony counting assay, biofilm formation assay supported the potent antimicrobial efficacy of b-Cs-AgNPs alone and when coated to medical grade catheters. Mechanistic studies reveal the presence of ferulic acid, that was important for the synthesis of b-AgNPs along with enhanced antibacterial effects of b-Cs-AgNPs compared to c-AgNPs, supported by molecular docking analysis. These results together demonstrated the effective role b-Cs-AgNPs in combating infections and mitigating biofilm formations, highlighting their need for further study in the field of biomedical applications.

Graphical abstract

Schematic Illustration of Eco-Friendly Synthesis for Biofilm Prevention on Medical Catheters and Bacterial Infection Mitigation. Created with BioRender.com.

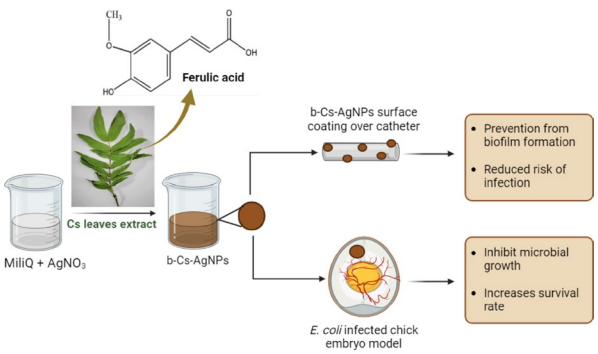

Keywords Biosynthesized silver nanoparticles (b-Cs-AgNPs) · Antibiofilm · Antibacterial · Medical catheters · Molecular docking

Lipi Pradhan and Prince Sah have contributed equally to this work.

Extended author information available on the last page of the article

Introduction

Medical devices have become an indispensable tool in the dynamic area of healthcare facilities. They have narrowed down the gap between advanced medical research and efficient patient care revolutionizing medical practices. Medical devices include a diverse array of equipment that spans from diagnostic and therapeutic instruments to monitoring and implantable tools. The invention of the latest medical devices has dramatically shifted the way of carrying out healthcare practices [1, 2]. They contributed to more precise diagnoses, reduced invasiveness, and improved patient health. However, a serious challenge associated with their transformative potential is the risk of bacterial infections. Patients face various complications due to infections acquired during their hospital stays. More than 700,000 individuals in the United States are affected by bacterial infection annually, resulting in significant rates of illness and even mortality [3, 4]. It has been reported that the majority of these healthcare-associated infections are closely related to medical devices, including ventilators, injectors, catheters, and implantable devices [4]. It is estimated that nearly 80% of these healthcare-acquired infections are linked to biofilm deposition. Catheter-associated urinary tract infections (CAUTIs) are the most frequent types of infections seen among patients [5–7]. Treatment of such infections pose a significant difficulty due to the potential growth of biofilms over the surface of medical devices [8]. Biofilms can be defined as tiny groups of microbial cells that can attach to surfaces and secrete a protective covering, preventing themselves from antibacterial agents and host's immune cells [9]. These biofilms acts as primary source infections in healthcare settings, posing a great risk to patients' safety [10]. Majority of the medical devices are made up of durable, polymer-based, hydrophobic materials including polyurethane, poly methyl methacrylate (PMMA) silicone rubber, etc. Polymer-based materials quickly get covered by biological liquids, like plasma proteins, providing a conducive environment facilitating biofilm growth and development. Once bacteria gets attached to these surfaces, it becomes very difficult to stop them from proliferating and forming biofilms [11]. Administrating significant amount of antibiotics or replacing the implant implies expensive and complex operations, both of which are ineffective because of antibiotic-resistant strains and have a substantial chances of reinfection on the replaced implant [12]. Currently, researchers are paying a great interest in developing antimicrobial coatings to improve the compatibility of medical devices and implants [13, 14]. Yet, these coatings have significant drawbacks, including biocompatibility and the inability to effectively combat multiple drug-resistant bacteria [15]. Researchers are exploring alternative strategies to overcome these challenges which includes use of antibacterial nanoparticles (NPs) like silver nanoparticles (AgNPs). AgNPs are widely recognized for their antibacterial and antibiofilm property [16, 17]. They exhibit diverse and multifaceted mechanisms to inhibit bacteria growth. They can generate reactive oxygen species, disrupt bacterial cell membranes, denature proteins, damage DNA, inhibit enzymes, release antibacterial ions, and interfere with quorum sensing systems preventing bacterial infections [18–20]. Additionally, AgNPs are biocompatible which indicates they are safe for use in various biomedical applications, minimizing risks to humans and the environment as a whole [21, 22].

In this research work, we employed an environmentally friendly green synthesis approach to create silver nanoparticles (b-Cs-AgNPs) utilizing the leaf extract of *Calliandra surinamensis* commonly referred to as pink powderpuff. It is a large, numerous-trunked, low-branching (Cs) perennial shrub generally found in subtropical and tropical regions of Asia, Africa, America, and Australia [23]. Cs is extensively studied for its antibacterial, anti-inflammatory, antidiabetic, antioxidant and wound-healing properties [23–26]. As per our knowledge, there have been no published reports of AgNPs synthesis involving leaf extract of Cs. Several characterization techniques such as DLS, TEM, UV–Visible spectroscopy, XRD, FTIR have been utilized to characterize b-Cs-AgNPs. We performed a chorioallantoic membrane (CAM) assay, MTT assay and skin irritation test using b-Cs-AgNPs confirming the biocompatibility in different living system. Moreover, the antimicrobial abilities of the b-Cs-AgNPs were evaluated by assessing the zone of inhibition and colony counting assay. To investigate the possibilities of b-Cs-AgNPs in preventing bacterial growth, we coated medical grade barium impregnated silicone rubber catheters with b-Cs-AgNPs using plasma activation. There after we conducted an antibiofilm experiment to study the impact of b-Cs-AgNPs on biofilm development. It was observed that b-Cs-AgNPs effectively prevented biofilm deposition on the surface of coated catheters. To further explore the effectiveness of b-Cs-AgNPs against infection, alginate discs were prepared by incorporating b-Cs-AgNPs. These discs were then implanted into an *E. coli* infected 4-day-old chick embryo model. The findings indicated that b-Cs-AgNPs discs successfully prevented bacterial growth compared to the untreated egg. These results reveal valuable insights into the potential application of b-Cs-AgNPs in fighting infections and preventing biofilm deposition.

Materials and methods

Chemicals

Silver Nitrate ($AgNO_3$) and Osmic acid were obtained from Central Drug House, Daryaganj, Delhi, and were used without any additional processing. Nitric acid (HNO_3), sodium borohydride ($NaBH_4$), sodium phosphate dibasic, hydrochloric acid (HCl), ferulic acid, sodium phosphate monobasic, fetal bovine serum (FBS), dimethyl sulfoxide (DMSO), phosphate buffer saline (PBS), trypsin EDTA, 3-(4,5-dimethylthiazol-2-yl)-2,5-diphenyl tetrazolium bromide (MTT) dye, crystal violet, Dulbecco's modified Eagle's medium (DMEM), acetic acid, alginate, glutaraldehyde, 4′,6-diamidino-2-phenylindole (DAPI) were obtained from SRL (Sisco Research Laboratories Pvt. Ltd.)—India. Calcium chloride ($CaCl_2$) sodium chloride (NaCl), were purchased from Thermo Fisher Scientific India Pvt. Ltd. HEK-293 (Human embryonic kidney) cells were procured commercially from the National Centre for Cell Science (NCCS), Pune. LB broth and LB nutrient agar were ordered from HiMedia Laboratories Pvt. Ltd. Barium impregnated medical silicone rubber catheters (Codman HOLTER Atrial Distal catheter, 821,670) were used for antibiofilm studies. GFP tagged *E. coli* was a generous gift from Prof. Bama Charan Mondal, BHU, Varanasi.

Calliandra surinamensis (Cs) leaf collections

C. surinamensis is an evergreen tropical shrub belonging to family Fabaceae. It is commonly named as Suriname powder puff or pink powder puff. As per published literature a heat-resistant lectin (CasuL) is found in the leaflets of Cs that shows cytotoxic, antibiofilm, and antifungal properties [25]. Additionally Cs has elements like saponins, tannins, and flavonoids that prevents microbial growth and development [27]. Various compounds including myricitrin, lupeol, and ferulic acid is reported in Cs plant. Myricitrin is noted for its anti-inflammatory and antioxidant properties [28]. Lupeol is recognized for its potential in combating inflammation and cancer [29], whereas ferulic acid is acknowledged for its antimicrobial properties. The aqueous extract of Cs leaves contains ferulic acid (FA), which aids in the reduction of silver and the formation of silver nanoparticles due to the presence of phenolic OH. In addition, FA contains negatively charged groups like carboxylate (COO^-) as well as polar molecules like OH, which have a strong inclination for forming ionic interactions with the Ag^+ ions, helping in the stabilization of the formed b-AgNPs [30]. The reason behind selecting Cs for our study is due to their antibacterial and antibiofilm activity. Moreover, there are no reports of nanoparticles being synthesized using Cs. We have collected Cs leaves from the campus of Banaras Hindu University, Varanasi, Uttar Pradesh, India. We employed Cs leaf extract as stabilizing and reducing agent in preparing biocompatible b-Cs-AgNPs utilizing an easy, ecofriendly green synthesis approach.

Bacterial strain

We used *E. coli,* strain *Dh5alpha* to study the antibacterial activity of b-Cs-AgNPs. GFP-*E. coli* was used for confocal microscopy.

Stock solution preparation for the nanoparticle synthesis

b-Cs-AgNPs were synthesized by the interaction of $AgNO_3$ solution. Autoclaved milliQ water was utilized to prepare 10^{-2} (M) of $AgNO_3$ stock solution [31].

Preparation of aqueous extract using *Calliandra surinamensis* leaves

Twenty gram of *Calliandra surinamensis* (Cs) leaves were collected as mentioned earlier. Leaves were then washed twice using 250 mL of miliQ. These washed leaves were then collected in a 500 mL beaker. 100 mL of autoclaved miliQ water was then added to the leaves and microwaved thrice for 1.30 min using a domestic microwave oven at 800 W. The sample containing leaves was then stirred for 10 min using a magnetic stirrer at 385 rpm. The sample was again microwaved for 2.30 min at 800 W followed by overnight stirring. Pale yellow colored extract was obtained which was collected in falcon tubes. This extract was then subjected to centrifugation at 7830 rpm for 30 min at room temperature. The supernatant formed was then collected and stored in −20-degree temperature for further studies.

Biosynthesis of silver nanoparticles (b-Cs-AgNPs)

We have chosen an environment friendly, green synthesis approach to create silver nanoparticles (b-Cs-AgNPs). For the synthesis of b-Cs-AgNPs, we employed silver nitrate ($AgNO_3$) as precursor, aqueous extract of Cs leaves served as reducing and stabilizing agents and autoclaved miliQ was the solvent. b-Cs-AgNPs were synthesized using four different reaction conditions, as shown in Table 1, keeping the volume of $AgNO_3$ constant. 200 µL of 10^{-2} (M) of $AgNO_3$ was mixed with appropriate amount of autoclaved miliQ (as per Table 1) and stirred for 2 min. Thereafter, different volumes of Cs leaf extract (250–1000 µL) were

Table 1 Various reaction conditions for synthesis of b-Cs-AgNPs

Exp no	Extract (µL)	10^{-2} M $AgNO_3$ (µL)	MiliQ (mL)	Total vol. (mL)
S1	250	200	4.55	5
S2	500	200	4.3	5
S3	750	200	4.05	5
S4	1000	200	3.8	5

added to the solution dropwise in stirring conditions. The resulting solution was allowed to stir for 8 h using a magnetic stirrer. Based on the concentration of Cs extract, the color of the solution changed from light yellow to dark brown. Four separate reactions were carried out, increasing the concentration of Cs leaf extract, to investigate the impact of b-Cs-AgNPs' size, shape, and surface characteristics on their antibacterial and antibiofilm capabilities. We employed TEM and DLS, respectively, to assess the synthesized NPs' size, shape, and surface charge.

Chemical synthesis of silver nanoparticles (c-AgNPs)

We synthesized c-AgNPs (Chemically synthesized silver nanoparticles) to examine the biocompatibility, antibacterial and antibiofilm properties of b-Cs-AgNPs in contrast to c-AgNPs. In order to synthesize c-AgNPs, 150 µL of 10^{-2} (M) of $AgNO_3$ was blended in 2.05 mL of autoclaved miliQ water employing magnetic stirrer. The formed solution was than reduced employing 2.8 mL of a $NaBH_4$ (0.05 mg/mL) solution resulting in dark grey colored c-AgNPs.

Preparation of b-Cs-AgNPs pellets

To prepare the sample for characterization process, 50 mL of b-Cs-AgNPs were centrifuged at 7830 rpm for 40 min at 25 °C using the 5430 R-High speed centrifuge. The resulting dark brown color pellet formed after centrifugation, was carefully collected. The resulting pellet was employed for subsequent characterizations, as well as for carrying out in vitro and in vivo experiments.

Characterization studies

Various characterization techniques were employed to gather vital information regarding the properties and behavior of synthesized b-Cs-AgNPs. The detailed process of characterization is provided in supporting information.

In vitro stability study

The stability of b-Cs-AgNPs were determined through an in vitro water dilution kinetic study. 100 µL of autoclaved Mili-Q was added step by step, to 1 mL of b-Cs-AgNPs to initiate the study. After every step we measured absorbance at 425 nm. Meanwhile, we also observed the stability of b-Cs-AgNPs in various solutions, including 1% NaCl, 5% NaCl, 10% NaCl, and phosphate-buffered saline adjusted to pH levels of 5, 6, 7, and 8. To determine the stability in different conditions, 100 µL of each solution was mixed with 900 µL of b-Cs-AgNPs. This mixture was allowed to incubate at room temperature for 48 h. The stability of b-Cs-AgNPs was observed through spectral scanning within the range of 290–500 nm using microplate reader. (Synergy H1-Microplate reader). We compared the stability of b-Cs-AgNPs with chemically synthesized AgNPs (with commercial quality) over an extended period of 3 months. Initially, the hydroscopic diameter of both b-Cs-AgNPs and c-AgNPs were measured using DLS after 24 h of synthesis. The diameter of 3-month-old AgNPs were further analyzed to check the change in size distribution and aggregation tendency.

DPPH assay

DPPH assay is widely used to check the antioxidant capacity of a sample. DPPH a purple-colored dye becomes colorless while reacting with antioxidants [26]. 0.78 mg of DPPH was weighed and dissolved in 10 mL of 99.5% ethanol. The resulting mixture was wrapped using aluminum foil and then kept for 2 h in the dark. b-Cs-AgNPs (30 µM), c-AgNPs (30 µM), and Cs (500 µL) were collected in eppendorf tubes. The samples were then diluted using miliQ water to prepare a 1 mL solution. 1 mL of already prepared DPPH solution was then added to these samples. The samples were kept in the dark for 30 min at room temperature allowing DPPH to react. Following 30 min incubation, absorbance of each sample was recorded at 517 nm using a bio spectrophotometer, keeping DPPH solution as control [32]. To quantify the scavenging activity, the percentage of inhibition is measured with help of given formula:

$$\%\ \text{of scavenging}\ \textit{activity} = \left(\frac{\text{Ac} - \text{As}}{\text{Ac}}\right) \times 100$$

where As denotes the absorbance of the sample, and Ac denotes the absorbance of the control (DPPH solution) at 517 nm.

Chorioallantoic membrane (CAM assay) to assess the biocompatibility of b-Cs-AgNPs

In this study, we used the CAM assay to examine the biocompatibility of b-Cs-AgNPs on development of blood vessels. To carry out this assay fertilized eggs were purchased from a hatchery located in Varanasi, Uttar Pradesh. The eggs were then kept at 37 °C for 4 days in an egg incubator. On fifth day, to visualize the developing blood vessels, a small opening was made on the outer shell of egg. Filter paper discs obtained from Whatman filter paper were incubated with the Cs extract (0.42 mg/mL) and b-Cs-AgNPs (~8 µM) for 2 min at room temperature. These discs were then carefully positioned on the blood vessels of the CAM layer. Using a stereo microscope (Magnus MagZoom TZM6 Trinocular Stereo Zoom Microscope), the effects of b-Cs-AgNPs on the growth and development of the blood vessels was monitored up to 6 h. Untreated eggs served as control sample [33].

Cell viability study employing MTT assay

MTT assay was conducted to examine the effect of b-Cs-AgNPs on the viability of the human embryonic kidney 293 cell line (HEK-293). 96-well plates were seeded with 1×10^4 Cells/100 µL. After 24 h, c-AgNPs and b-Cs-AgNPs were added as treatments at three different concentrations (27.5, 41.25 and 68.75 µM) and incubated for 24 h. Following the removal of the medium, 100 µL (0.5 mg/mL) MTT suspension was added, and the resulting mixture was incubated for 4 h at 37 °C in an incubator with 5% CO_2. Subsequently, 100 µL of DMSO:MeOH (1:1) was added in order to break down the formazan crystal after the MTT solution had been gently removed. The absorbance of the mixture was analyzed using a multiplate reader at 570 nm. Thereafter, the cell viability (%) was calculated using the following formula:

$$\% \text{ cell viability} = \left(\frac{\text{As}}{\text{Ac}}\right) \times 100$$

As and Ac denotes absorbance of sample and control at 570 nm.

Skin irritation test to examine effect of b-Cs-AgNPs on rat model

Dermal skin irritation study was performed after IAEC approval (IIT(BHU)/IAEC/2023/068; Approval Date: February 9, 2023). Healthy Wistar rats (6–8 weeks old; 150–175 g) were obtained from CDRI-Lucknow and employed for in vivo skin irritation experiment. We performed a skin irritation test to evaluate the effect of b-Cs-AgNPs on the skin of rat. Initially we shaved the fur of rat and applied 0.8% formaldehyde, which is a commonly used irritant over the naked skin. The skin of another rat was treated with b-Cs-AgNPs. The skins were exposed to these samples for 7 days and images were captured at different time point to check any inflammatory reactions.

Antibacterial study

We conducted the following three experiments to study the antibacterial activity of b-Cs-AgNPs.

Bacterial growth inhibition (BGI)

The effects of b-Cs-AgNPs on bacterial growth and proliferation was assessed in LB (Luria–Bertani) medium. First, *E. coli* cultures were inoculated into LB medium and kept overnight at 37 °C. Next day, the bacterial culture was combined with fresh LB medium and allowed to incubate until the optical density (OD) reaches 0.6. The OD of 0.6 was confirmed by measuring the absorbance of medium at 600 nm. 20 mL of LB media was collected in each test tube. These media were blended using various concentration of b-Cs-AgNPs, c-AgNPs, Cs and ampicillin. 200 µL of freshly cultured *E. coli* (approximately, OD = 0.6) were introduced to each media [34]. To monitor the growth of *E.coli* in different medium, absorbance was measured at 600 nm up to 8 h using a microplate reader (Synergy H1-Microplate reader).

Agar disc diffusion method

This method was utilized to evaluate the antimicrobial behavior of b-Cs-AgNPs against different bacterial strains. Initially, both *E. coli* (gram negative) and *Bacillus subtilis* were allowed to grow until the OD reaches nearly 0.6. Initially, 200 µL of freshly cultured bacterium were plated under sterile conditions. Pre-sterilized filter paper (Whatman no. 1) discs were soaked in the b-Cs-AgNPs, c-AgNPs solution and an antibiotic (Ampicillin, 1 mg/mL) solution for 15 min. These soaked discs were then placed carefully on top of the agar plates. Following this, the agar plates were allowed to incubate for a duration of 24 h at 37 °C. The zone formed around the discs was then quantified to determine the antimicrobial potency of given sample.

Determination of colony forming units

The colony counting method serves as a reliable approach in determining a bacterium's capacity of forming colonies when subjected to any kind of treatment. Two different concentrations of b-Cs-AgNPs (30 µM and 50 µM) were blended with 20 mL of LB agar medium. After that, 200

µL of freshly prepared *E. coli* cultures (OD ≈ 0.6) were introduced onto the agar plates. Ampicillin (30 µM) was employed as a positive control, and c-AgNPs (30 µM) were used to compare the antibacterial effects of b-Cs-AgNPs. These agar plates were kept in an incubator for a day at 37 °C temperature. Following incubation period, the number of colonies formed on the surface of the LB agar plates was assessed using ImageJ software.

2.16 In ovo study for mitigation of bacterial infection in chicken egg model

Preparation of anti-bacterial alginate disc

To explore the potential of b-Cs-AgNPs in an *E. coli*-infected chick embryo model, three different types of alginate discs were made and compared with c-AgNPs. Initially, 70% low-density alginate was mixed with 30% high-density alginate. The solution was allowed to stir for 5 min using a magnetic stirrer. 30 µM of b-Cs-AgNPs were mixed to the solution and stirred for 30 min to blend the mixture. The resulting solution was poured in a circular mold created using 3D printing technology. The mold was then immersed in a $CaCl_2$ crosslinking solution to form an antimicrobial alginate disc with a diameter of 10 mm. Similarly, c-AgNPs alginate discs were also prepared. No NPs were utilized in the preparation of untreated discs (Supporting Fig. 4).

In ovo CAM infection with *E. coli*

On fifth day of incubation, the chicken eggs were infected by applying 100 µL (OD = 0.6) of *E. coli* bacterial inoculum, avoiding dispersion of the inoculum too close to the developing embryo. These infected eggs were then divided into three distinct groups. In the first group, the infected eggs were treated using b-Cs-AgNPs containing alginate discs. The second group received c-AgNPs alginate discs, while the third group was treated with alginate discs only. Microscopic images were captured at various time intervals over a period of 4 h to observe the development of blood vessels using a stereo microscope (Magnus MagZoom TZM6 Trinocular Stereo Zoom Microscope). After the 4-h, 50 µL of allantoic fluid was collected using pipette, diluted fivefold using autoclaved miliQ, plated, and placed at 37 °C for 24 h to determine the presence of infection [35].

2.17 Antibiofilm study

Antibiofilm surface coating on medical catheter

Medical catheters were coated applying both chemically and biologically synthesized NPs to assess their antibiofilm properties. Initially, barium-impregnated silicone rubber catheter (specifically, Codman HOLTER Atrial Distal catheter, 821,670) [36], was subsequently cut into smaller pieces measuring 0.5 cm each. We treated these pieces using plasma (Plasmasystem Zepto One) for 5 min to enhance the bonding between the NPs and the catheter. The plasma treatment improved the surface energy of the catheter, ensuring a stronger bond with the subsequently applied coatings material. The catheter segments were submerged in a concentrated solution of b-Cs-AgNPs and c-AgNPs soon after the plasma treatment. The samples were then kept on a magnetic stirrer overnight to facilitate the final coating of the NPs on the surface of catheters.

Biofilm deposition on catheters

To examine the antibiofilm property of synthesized NPs, bacteria were allowed to grow and form biofilm on the surface of catheters. Initially, *E. coli* was cultured until the optical density (OD) reached 0.6, assuming the bacterial culture had reached its log phase. Following this, 3 mL of LB (Luria–Bertani) media was added to each well of a 6-well plate. 30 µL of freshly cultured *E. coli* were inoculated in each well. Subsequently, the NPs coated catheters were carefully placed into these wells. The plates were then kept at 37 °C in an incubator for 48 h allowing biofilm to grow over the medical catheters.

Crystal violet staining assay

We allowed the biofilm to grow over the medical catheter (as discussed earlier). After 48 h of incubation, we washed the catheter twice using PBS buffer to remove any loosely attached bacteria. The catheter was then left to air dry for 15 min. 200 µL of a 0.1% solution of crystal violet (CV) stain was added to the catheter to assess biofilm's biomass. The staining process was carried out for 40 min while the catheter was gently rocked at a rate of 10 oscillations per minute. After the staining step, catheter was gently washed with PBS to get rid of any unbound stain. The catheter was allowed to air dry for 3 h. The biofilm was then fixed with 200 µL of a solution containing 80% ethanol and 20% acetone. The catheter was gently rocked for 10 min to ensure even distribution of the fixative agent. Absorbance of the CV stained biofilm was recorded at 595 nm to measure the biofilm biomass [37].

We calculated the % of biofilm inhibition using the following formula:

$$\%\ \text{of biofilm inhibition} = \left(\frac{\text{Ac} - \text{As}}{\text{Ac}}\right) \times 100$$

Ac denotes the absorbance of the control whereas as denotes the absorbance of the sample at 595 nm.

Confocal microscopy analysis to assess the anti-biofilm properties of b-Cs-AgNPs

Initially, a small piece of medical catheter was allowed to deposit biofilm in presence of LB media for 2 days. After the incubation period, the LB media were collected in an eppendorf tubes. These media were centrifuged for 15 min at 13,000 rpm. The resulting pellet was collected and washed twice using PBS buffer. After washing the pellet was stained using 200 µL of DAPI (15 µg/mL) solutions to visualize the biofilm. Following DAPI staining the pellet was washed with PBS buffer to eradicate unbound molecules. Thereafter, 10% formalin was utilized to fix the pellet to a glass slide and allowed to dry for 30 min at room temperature. Following the fixation step, images were captured utilizing a confocal microscope (Zeiss 510 Meta confocal microscopy system).

Reusability study to identify antibiofilm properties of b-Cs-AgNPs coating over prolonged use

Initially, we incubated b-Cs-AgNPs coated and uncoated catheter with GFP *E. coli* (OD approx. 0.6) for 24 h. Following the incubation period, the fluorescence intensity (Excitation wavelength = 485 nm, emission wavelength = 528 nm) of the bacterial suspension was measured using a multiplate reader. The experiment was repeated twice to check the reusability of b-Cs-AgNPs coated catheters.

Effect of b-Cs-AgNPs in extracellular polymeric substances (EPS) of bacterium

We analyzed the effect of b-Cs-AgNPs in extracellular polymeric substances (EPS) of bacterium to study antibiofilm effects. We allowed two different strains of bacteria, *B. subtilis* and *E. coli* to grow until the OD reaches 0.6. 20 µL of inoculum was added to 2 mL LB broth in 6 well plate. 30 µM b-Cs-AgNPs was treated to each well. Untreated bacteria served as control. The samples were incubated for a day at 37 °C on a shaking incubator. After 24 h, bacterial culture was centrifuged at 6000 rpm for 30 min at 4 °C and the supernatant was collected. Two volumes of acetone were added to the supernatant, and the mixture was refrigerated overnight (at 4 °C) for the precipitation of EPS. EPS product was finally collected by centrifugation of the mixture at 6000 rpm for 30 min (at 4 °C) to collect pellet. Wet weight of the pellet was measured [38].

SEM analysis to study the ability of b-Cs-AgNPs to disrupt mature biofilms formed by various bacterial strains

Initially, we cultured *E. coli* and *B. subtilis* on a glass coverslip for 24 h to facilitate the development of mature biofilm. Following a day, we introduced 150 µL of b-Cs-AgNPs into the developed biofilm and allowed it to react for an additional 24 h. The coverslips were examined under a SEM after being fixed with glutaraldehyde.

Unlocking the possible mechanism of FA as reducing and antimicrobial agent of b-Cs-AgNPs

Synthesis of b-Cs-AgNPs employing FA as reducing agent

To evaluate the role of bioactive compound present in leaf extract of Cs, we took 4 mL of silver nitrate (10^{-2} M) solution in a glass beaker. 1 mL of ferulic acid (1 mg/mL) was added to the $AgNO_3$ and placed at a hot plate magnetic stirrer for 4 h, keeping the temperature at 40 °C. After 4 h, the color change was observed from transparent to pale yellow, suggesting the formation of AgNPs. Moreover, UV and DLS studies were performed to confirm the synthesis of AgNPs.

Antibacterial activity of ferulic acid

It has been reported that Cs contains ferulic acid, which exhibits antimicrobial properties. To check the efficacy of ferulic acid (FA) in inhibiting the growth of *E. coli*, a biofilm growth inhibition (BGI) assay was conducted. For this purpose, 3 mL of Luria–Bertani (LB) broth was dispensed into each well of a 6-well plate. Subsequently, 30 µL of *E. coli* culture (OD-0.6) was poured to each well. Two distinct concentrations of ferulic acid (0.5 mg/mL and 1.0 mg/mL) were introduced into the solution. The 6-well plates were subsequently maintained in an incubator for a day at 37 °C. Following the incubation period, the absorbance of the samples was recorded at a wavelength of 600 nm.

Molecular docking analysis understanding the mechanism of antibacterial and antibiofilm properties of b-Cs-AgNPs

Two softwares OpenBabel and AutoDock were used to perform docking analysis. Initially, OpenBabel software was employed to download ferulic acid compound from PubChem in ".sdf" format and then converted it to ".pdb". AutoDock was used to initiate the process of docking. First of all, the ligand for docking was generated by adding hydrogen atoms and gasteiger charges. The proteins essential for stimulating biofilm formation and survival of *E. coli* were used as receptors. X-ray crystallographic structures of these crucial proteins which includes DNA gyrase (pdb id: 1KZN), FabH (pdb id: 1EBL), DosC (pdb id: 4ZVF), and PgaB (pdb id: 4P7O) were collected from PDB database. These obtained proteins were further converted into ".pdbqt" format with the help of OpenBabel. All the water molecules in pdb files were eliminated to remove unfavorable atoms present on receptors. Moreover, applying AutoDock we attached Kollman charge (surface charge) along with polar

hydrogens to the backbone of these receptors. To facilitate the docking process of above listed proteins the grid spacing of 3D grid box was adjusted at 0.375. Automated molecular docking was performed using LGA (Lamarckian genetic algorithm) [39].

Statistical analysis

The experiments were conducted trice to ensure accuracy and reliability. The data from each experiment were expressed as the mean value and standard error. With the use of the Origin software, a one-way ANOVA was carried out to determine the statistical significance of observed data.

Results and discussion

Synthesis and characterization of biosynthesized silver nanoparticles

The utilization of a green, sustainable agent and a straightforward, one-step reaction procedure makes the biological production of silver nanoparticles a superior method compared to current techniques. $AgNO_3$ and various amounts of Cs extract were used to synthesize b-AgNPs (as stated in Table 1). A number of reactions were conducted to establish the ideal conditions for production of b-Cs-AgNPs. By altering the amounts of miliQ water and Cs extract, the reaction mixture's overall volume was kept at 5 mL, while the amount of $AgNO_3$ (200 µL of 10^{-2} M) was kept constant. Experiment S2 in Table 1 demonstrates the optimal conditions for formation of b-Cs-AgNPs-500, achieving a 2-h reaction duration. The emergence of a yellowish color in the reaction mixture served as a precursor to the synthesis of AgNPs (Supporting Fig. 1a) which was later validated by several physicochemical methods. A dark brown color was observed after 8 h of synthesis (Supporting Fig. 1b) indicating the formation of silver nanoparticles.

The absorbance of all the reaction sets were recorded after 8 h of synthesis using UV–visible spectroscopy, as depicted in Fig. 1a. The presence of the optimized b-Cs-AgNPs was confirmed by observing the UV absorption peak of AgNPs, which was detected at approximately 382 nm (Fig. 1a). This finding aligns with previously published reports and provides evidence of the successful formation of b-Cs-AgNPs in the pellet [40]. The presence of a shoulder around 380 nm in the spectrum suggests that it could be caused by tiny, isolated spherical nanoparticles measuring less than 10 nm in size [41]. The higher UV absorbance observed in S2 (b-Cs-AgNP-500) indicates an enhanced production of b-Cs-AgNPs and an amplified intensity of the absorption peak. Consequently, the b-Cs-AgNPs derived from reaction S2 are deemed as optimized nanoparticles. These optimized nanoparticles will be employed for all subsequent characterization techniques and for conducting both in vitro and in vivo studies. During the continuation of experiment S2 (b-Cs-AgNP-500) for up to 24 h, we observed a progressive increase in absorbance intensity over time (as shown in Fig. 1b). A comparable pattern of absorbance changes over time was likewise observed in the experiments designated as S1, S3, and S4. Notably, it was found that after a specific duration, the intensity of absorbance reached a plateau, suggesting the completion of reduction process (Supporting Fig. 2a). The pH of b-Cs-AgNPs also remained same with time indicating the reaction stability (Supporting Fig. 2b).

Dynamic Light Scattering (DLS) is used to access size and charge of b-Cs-AgNPs, as shown in Fig. 1c–f, respectively. Table 2 illustrates the size variations observed in different reaction sets, with S2 being the optimized one. For the optimized b-Cs-AgNP-500, the hydrodynamic diameter measures at 85.37 nm (Fig. 1d). The diverse sizes of b-Cs-AgNP observed through DLS could be attributed to the presence of both potent and less potent reducing components in the Cs. It is studied that leaf extracts contain molecules with varying degrees of reducing power. This reducing power directly influences the sizes of nanoparticles formed during the synthesis procedure. Strong reducing compounds tend to produce significantly smaller nanoparticles [42]. The charge plays critical role in governing the dispersion of b-Cs-AgNPs. It serves as an indicator of the repulsion among NPs, which play a great role in stability for longer duration. In the case of b-Cs-AgNPs, the zeta potential value is negative (-47.77 ± 0.35 mV), indicating a stable nanoparticle formation without any aggregation (Table 2). Overall, the negative zeta potential is a crucial factor contributing to the long-term stability of b-Cs-AgNPs and their effective dispersion.

DLS data revealed the least hydrodynamic diameter for b-Cs-AgNP-250 and b-Cs-AgNP-500 among the four batches. The surface charge for all the batches were highly negative with b-Cs-AgNP-500 showing highest charge reflecting their colloidal stability. The structure, size, and shape, of b-Cs-AgNPs obtained after 1 day of reactions were further analyzed using Transmission Electron Microscopy (TEM). The TEM images revealed spherical-shaped NPs with metallic sizes less than 10 nm for all the four different groups (b-Cs-AgNP-250, b-Cs-AgNP-500, b-Cs-AgNP-750, and b-Cs-AgNP-1000) (Fig. 1g–j). Based on the TEM analysis, size of b-Cs-AgNP-500 is found in between 9–10 nm (Fig. 1h). The size measurements obtained for b-Cs-AgNPs in TEM are consistently smaller in comparison to the results from DLS (Fig. 1d). DLS determines the hydrodynamic diameter of b-Cs-AgNPs, considering the size of the nanoparticles as well as the presence of biomolecules and proteins that coat nanoparticles' surfaces during biosynthesis. Conversely, TEM gives the precise size of the metallic core

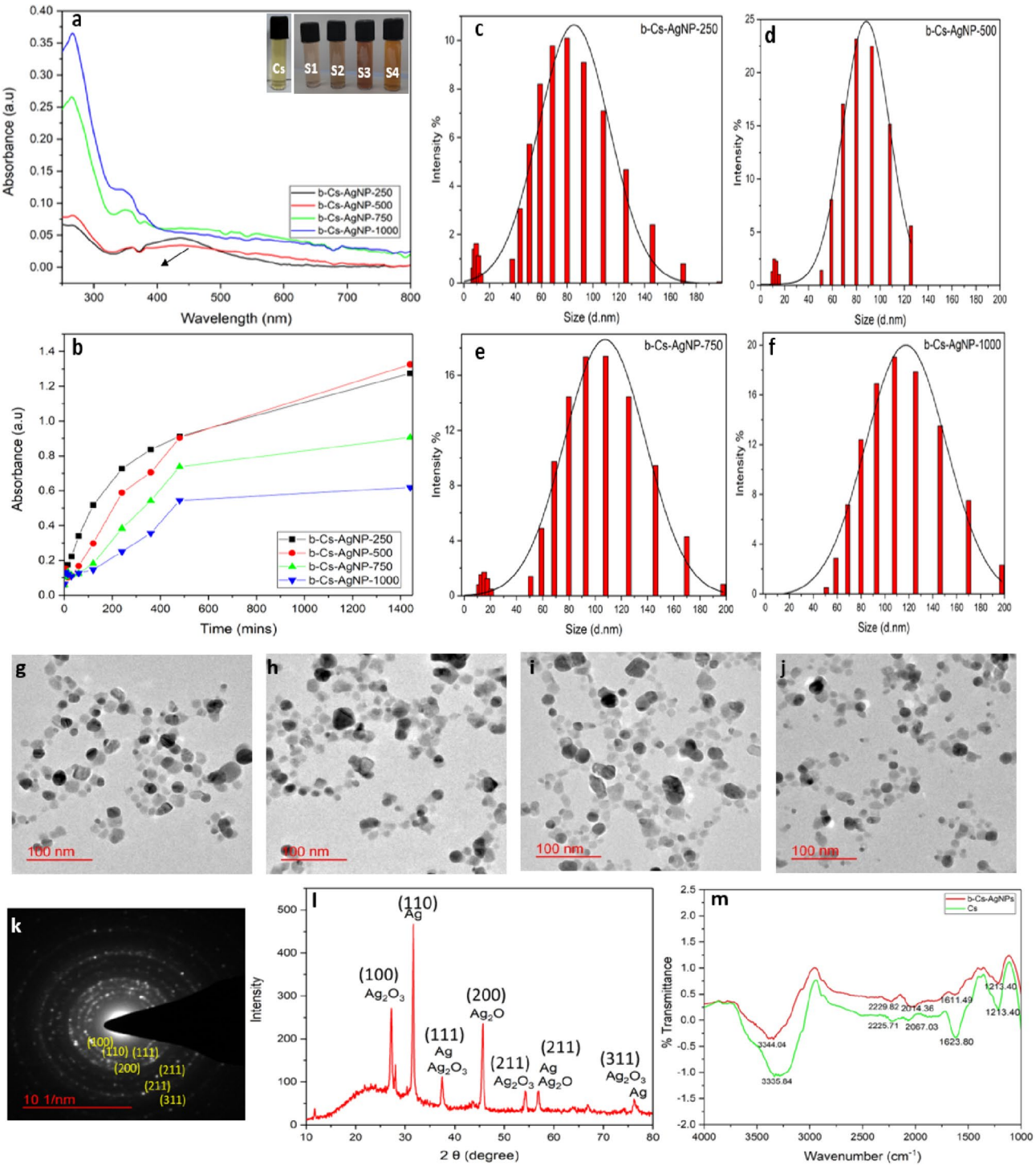

Fig. 1 Characterizations **a** UV–Visible spectra of biosynthesized silver nanoparticles (b-Cs-AgNPs) using different volumes of Cs extract (250–1000 µL), **b** Change of absorbance of different reaction conditions of b-Cs-AgNPs with time (0 min to 24 h), **c**–**f** Dynamic light scattering (DLS) distribution plot of b-Cs-AgNPs with varying volume of Cs. **g**–**j** TEM images of b-Cs-AgNP-250, b-Cs-AgNP-500, b-Cs-AgNP-750 and b-Cs-AgNP-1000, respectively, indicating spherical shaped NPs formed from all the four reaction conditions **k** SAED patterns confirm the face-centered cubic (FCC) lattice structure of b-Cs-AgNP-500, **l** X-ray diffraction patterns indicating FCC crystal structure of synthesized b-Cs-AgNP-500, **e** FTIR analysis of the b-Cs-AgNP-500 (top spectra) and Cs (lower spectra) exhibiting the functional groups involved in synthesis and stabilization of b-Cs-AgNP-500

Table 2 Size and charge of the b-Cs-AgNPs obtained from DLS study

Sample no	Sample name	Hydrodynamic diameter (nm)	Zeta potential (mV)
S1	b-Cs-AgNP-250	85.37 ± 1.37	−45.24 ± 0.14
S2	b-Cs-AgNP-500	88.24 ± 0.66	−47.77 ± 0.35
S3	b-Cs-AgNP-750	110.52 ± 1.14	−45.68 ± 0.34
S4	b-Cs-AgNP-1000	117.51 ± 1.00	−36.05 ± 0.28

of b-Cs-AgNPs excluding any attached biomolecules. The reaction stability, maximum silver nanoparticles production and effective antibacterial abilities are some of the key reasons to choose S2 (b-Cs-AgNP-500 denoted as b-Cs-AgNPs from now on) for remaining characterization, investigation of biocompatibility, stability, and in vitro and in vivo studies.

The inset in Fig. 1k displays the selected area electron diffraction (SAED) pattern of b-Cs-AgNP-500, showing Debye–Scherrer rings associated with the (100), (110), (111), (200), (211), (211), and (311) lattice planes of the face-centered cubic (FCC) structure, which aligns with the XRD pattern shown in Fig. 1l. X-ray diffraction spectroscopy (XRD) pattern of b-Cs-AgNPs exhibits seven distinct peaks at 2θ positions. In comparison to the standard spectra of silver (JCPDS file no. 04-0783) and silver oxide (JCPDS card no. 00-076-1393), the X-ray Diffraction (XRD) spectra (Fig. 1l) exhibit a strong resemblance. The prominent peaks in the pattern align with the Miller indices (hkl) characteristic of both silver and silver oxide, namely (100), (110), (111), (200), (211), (220), (310), and (311). Consequently, the XRD analysis confirms that the crystal structure of b-Cs-AgNPs is in the face-centered cubic (FCC) configuration supporting the SAED pattern [43, 44]. Fourier transformed infrared spectroscopy (FTIR) was employed to investigate the probable functional groups present in the Cs leaves important for the reduction of $AgNO_3$ to b-Cs-AgNPs and subsequently stabilizing them. Figure 1m displays the FTIR analysis of b-Cs-AgNPs (in red) and Cs leaves (in green), showing distinct IR peaks. The major IR stretching frequencies observed in Cs leaves were at 3335.84, 2229.82, 2014.36, 1611.49, and 1213.40 cm^{-1}. On the other hand, b-Cs-AgNPs exhibited IR peaks at 3344.04, 2225.71, 2067.30, 1623.80, and 1213.40 cm^{-1}. Upon investigating the FTIR spectra of Cs leaves extract corresponding to b-Cs-AgNPs, significant shifts in peak positions were observed, which can be reasonably attributed to the reduction, capping, and stabilization processes during the synthesis of nanoparticles [45]. The prominent peak at 3335.84 cm^{-1}, which corresponds to –OH stretching due to phenolic compounds present in Cs leaves, underwent a shift to 3344.04 cm^{-1}, demonstrating the role of phenolic compounds in the formation and stabilization of b-Cs-AgNPs [46]. The bands around 2229.82 and 2225.1 cm^{-1} were associated with the alkyne (C≡C) moiety present in the phyto-constituents of the extract. The peak at 2014.36 cm^{-1}, representing C–H stretching, shifted to 2067.30 cm^{-1} during b-Cs-AgNPs synthesis. Furthermore, the peak at 1611.49 cm^{-1} shifted to a higher wavelength of 1623.80 cm^{-1}, suggesting the involvement of alkenyl or aromatic C=C containing phytochemicals [47]. A possible explanation for the C-N stretching of the peaks designated at 1213.40 cm^{-1} is the possible existence of amine groups [47]. Therefore, the presence of phenols, alkynes, aromatic, and amine groups within the Cs leaf extract appears to be responsible for the formation of b-Cs-AgNPs. Further, we utilized ICP-MS analysis to determine the silver (Ag) concentration within b-Cs-AgNPs. Through the ICP-MS data, it was determined that the concentration of silver in b-Cs-AgNPs stands at 1.48 μg mL^{-1}.

In vitro studies showed excellent stability of b-Cs-AgNPs

Biomedical applications often require lower concentrations of b-Cs-AgNPs, making it crucial to ensure that the physio-chemical properties of the b-Cs-AgNPs solutions remain unchanged upon dilution. This indirectly indicates the in vitro stability of b-Cs-AgNPs. To assess the in vitro stability, a dilution kinetic study was conducted. The results revealed a linear correlation between the absorption intensity and the varying concentration of b-Cs-AgNPs, in accordance with the Lambert–Beer law (Fig. 2a). Importantly, the absorbance did not exhibit significant changes during dilution, indicating the superior stability of b-Cs-AgNPs. This finding supports the use of b-Cs-AgNPs in biomedical applications with confidence. Moreover, stability of b-Cs-AgNPs were tested in various phosphate buffer solutions with pH ranges from 5 to 8, and 5–10% NaCl solutions. Remarkably, after each incubation time point, we observed minimal changes in the absorbance indicating stability of silver NPs important for any biomedical applications (Fig. 2b, c).

Moreover, we compared the stability of b-Cs-AgNPs with c-AgNPs over an extended period of 3 months. Our findings demonstrated that, the average hydroscopic diameters of b-Cs-AgNPs and c-AgNPs after 24 h of synthesis were 88.24 ± 0.66 nm and 142.73 ± 1.82 nm, respectively, that has slightly changed after 3 months (b-Cs-AgNPs = 118.80 ± 0.03 nm, and c-AgNPs = 108.31 ± 0.90 nm) (Fig. 2d–g). In addition, c-AgNPs synthesized after a 24-h period had a surface charge of −8.01 mV, whereas b-Cs-AgNPs showed an elevated surface charge of −47.77 mV. However, after 3 months, notable alterations in the surface charge of both NPs were noticed. The surface charge for c-AgNPs decreased to −4.84 mV, as it became less stable over time. Similarly, the surface charge of b-Cs-AgNPs decreased, but it remained significantly higher

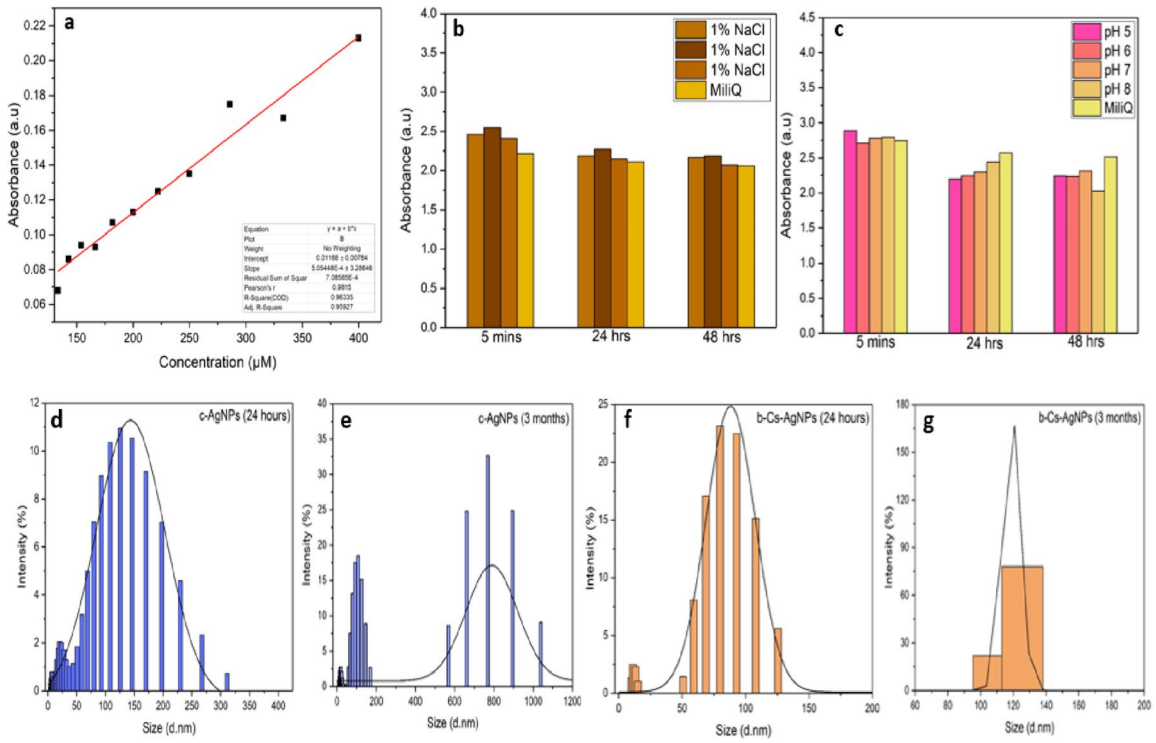

Fig. 2 **a** Change in the absorption of b-Cs-AgNPs under various dilution conditions with water. The linear fit supports the greater stability of b-Cs-AgNPs, **b**, **c** bar-diagram of in different b-Cs-AgNPs buffer solutions (0–48 h), **d**–**g** Dynamic light scattering (DLS) distribution plot of c-AgNPs and b-Cs-AgNPs obtained after 24 h and 3 months of synthesis

at −14.50 mV confirming colloidal stability. Results indicate that b-AgNPs can be equally, or better stable compared to the commercial chemical synthesized silver nanoparticles due to inherent presence of stabilizing phytochemicals.

To identify the stability of b-Cs-AgNPs coating over time we performed EDAX (Energy-dispersive X-ray spectroscopy) utilizing, EVO-Scanning Electron Microscope MA15/18, 51N1000—EDS System of freshly coated catheter and compared it with the 6 months old, coated catheter. The results in Supporting Fig. 3 demonstrated that negligible reduction in the silver content indicating excellent stability of the coating over time (the wt% of Ag was found to be 74.7% in freshly coated catheter with b-C-AgNPs and 65.4% in 6 months old catheter). Further the FE-SEM images confirmed the attachment of spherical shaped silver nanoparticles over catheters in both conditions supporting the coating stability over time (Supporting Fig. 3).

Antioxidant activity of b-Cs-AgNPs

The antioxidant potential of Cs, c-AgNPs and b-Cs-AgNPs were assessed using the DPPH free radical assays. In the DPPH assay, the reagent, when mixed with ethanol, results in a violet solution due to the exchange of free electrons. The introduction of an antioxidant leads to a color change from violet to colorless, indicating the absorption of free radicals by the antioxidant agent through hydrogen donation. The scavenging property of the formed AgNPs were assessed by observing a color shift from violet to yellow indicating the generation of diphenyl picryl hydrazine [48]. Among the studied samples, Cs demonstrated the highest capacity for reduction, displaying a scavenging efficiency of 90.3% at 4.6 mg/mL concentration (Supporting Fig. 4). The scavenging efficiency of b-Cs-AgNPs and c-AgNPs stood at 69.5% and 56.3%, respectively, at a concentration of 30 µm indicating strong antioxidant potential that is important for their overall biocompatibility and radical scavenging properties.

Biosynthesized silver nanoparticles demonstrated in vivo biocompatibility in chicken egg model

The CAM (Chorioallantoic membrane) assay is designed to assess the compatibility of nanomaterials with living tissue by observing changes in blood vessel junctions and growth. Chick embryo blood vessel images were captured at different time points up to 6 h after applying treatments, utilizing a stereo microscope (Supporting Fig. 5).

The results depicted in Fig. 3a–f reveal that b-Cs-AgNPs and Cs treatments did not hinder blood vessel formation or disrupt vascular structures in chick embryos. Moreover,

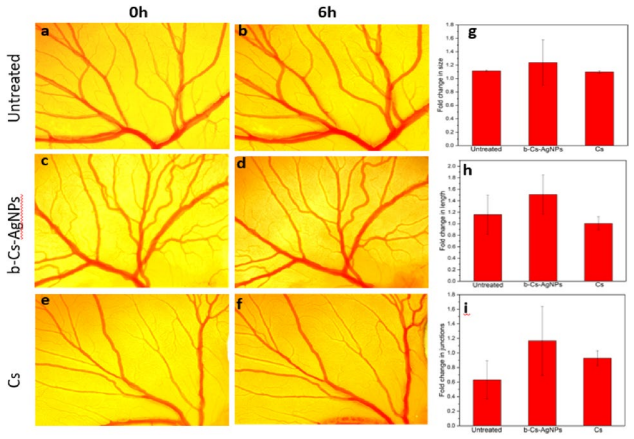

Fig. 3 CAM assay **a**–**f** shows the microscopic images of untreated, b-Cs-AgNPs, and Cs treated chick embryo models at 0 h and 6 h. **g**–**i** The images are quantified with respect to length, junction, and size using ImageJ and Angiotool software. These experiments are performed thrice and represented as mean ± SD. No significant differences from untreated embryos are observed (*$p > 0.05$)

Angiotool and ImageJ Software were employed for quantification of parameters related to blood vessel integrity, such as size, junctions, and length (Fig. 3g–i). The analysis indicated that the size remained relatively consistent across all samples. However, the length and junction parameters exhibited more significant changes compared to the untreated sample. This suggests the possibility of certain phytochemicals in Cs promoting the angiogenesis process. Overall, the results support the biocompatibility of the b-Cs-AgNPs important for biomedical applications.

MTT assay revealed b-Cs-AgNPs are non-toxic to human cell line even at higher concentration

MTT assay was conducted to examine the effect of b-Cs-AgNPs on the viability of the human cell line (HEK-293). The results of MTT assay demonstrated that, b-Cs-AgNPs did not show any notable cytotoxicity in different doses (27.5–68.75 µM). However, c-AgNPs restricted cell growth as dosage increased indicating cytotoxicity (Fig. 4a).

Skin irritation text revealed b-Cs-AgNPs does not cause any immune reactions when exposed to rat's skin

Skin irritation test is a widely employed study to investigate the inflammatory responses triggered by a sample following contact with the skin. It was observed that the skin exposed to formaldehyde showed redness after 24 h and the inflammatory response increased with subsequent uses and observance of hives at day 7 (Fig. 4b). In contrast, the skin exposed to b-Cs-AgNPs does not cause any

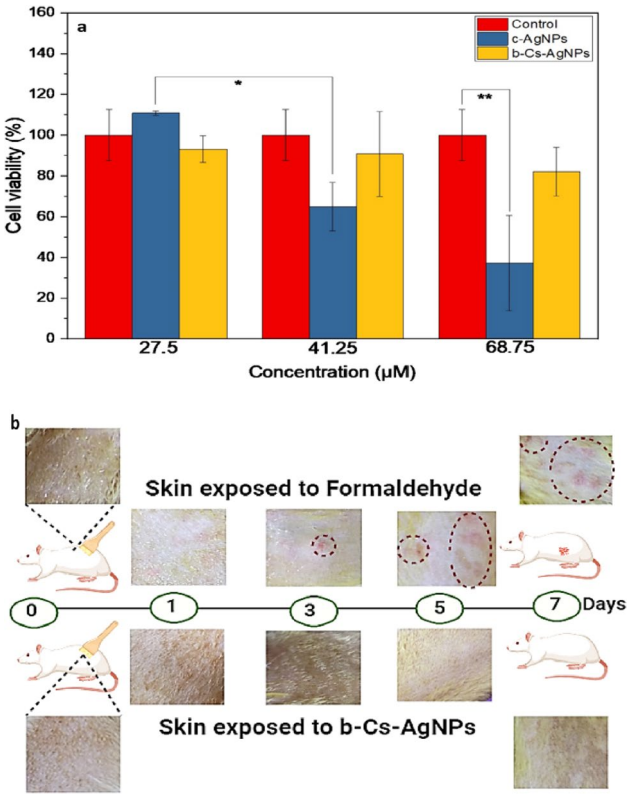

Fig. 4 **a** MTT assay showing b-Cs-AgNPs are non-toxic to cells even at higher dosage, **b** skin irritation test indicating b-Cs-AgNPs does not elicit immune response when exposed to rat skin

redness or hives suggesting b-Cs-AgNPs does not elicit skin irritation even after prolonged use.

b-Cs-AgNPs demonstrated potent antibacterial effects

Bacterial growth inhibition (BGI) studies showed anti-bacterial effects of b-Cs-AgNPs

A bacterial growth inhibition assay was performed to evaluate the antibacterial efficacy of b-Cs-AgNPs against standard antibiotics and c-AgNPs to compare the rate of bacterial inhibition (Fig. 5a). The nearly constant bacterial absorbance over the course of the experiment indicates that b-Cs-AgNPs (both 30 and 50 µM) and c-AgNPs (30 µM) exhibits a sustained inhibitory effect on bacterial growth and proliferation. The untreated sample shows sigmoid growth curve of bacteria (Fig. 5a). In contrast, antibiotic (ampicillin) treatment initially prevented bacterial growth. However, the bacteria growth slowly increased following 4 h indicating ineffective long-term treatment with similar doses (30 µM) [49].

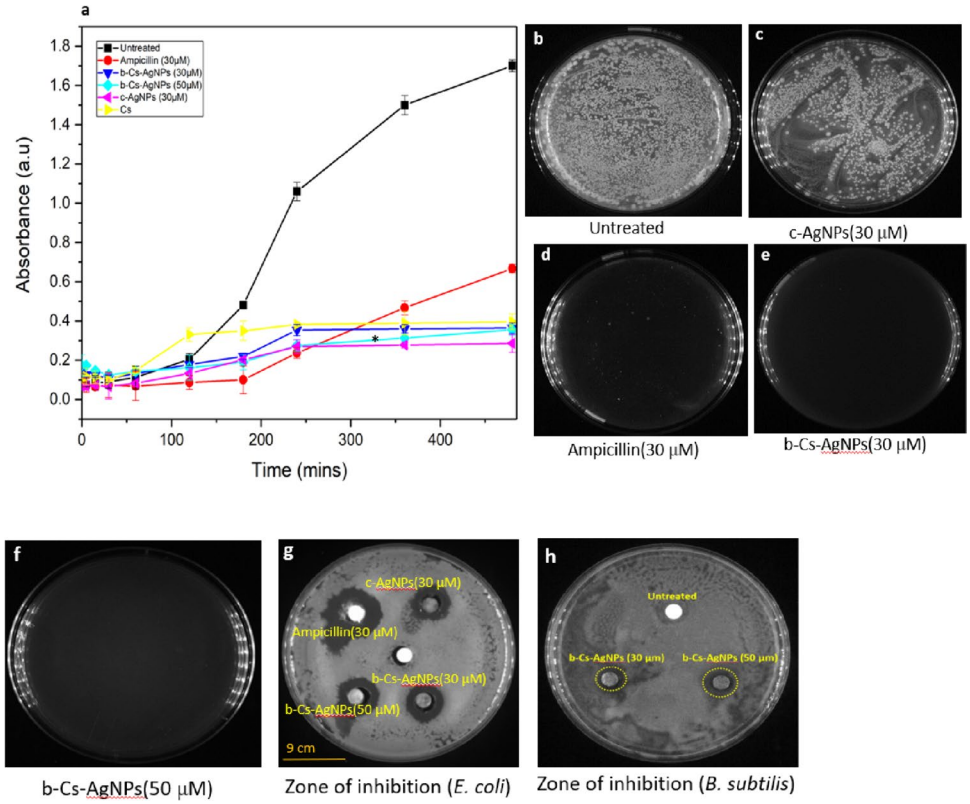

Fig. 5 **a** Growth curve of bacteria in presence of different concentration of b-Cs-AgNPs, c-AgNPs and Cs. Significant differences from untreated embryos are observed when treated with b-Cs-AgNPs (30 μM)(*$p < 0.05$), **b**–**f** Colony forming assay. **g**, **h** Zone of inhibition

Colony forming assay supported the anti-bacterial effects of b-Cs-AgNPs

The assessment of the antimicrobial effectiveness of b-Cs-AgNPs is achieved by quantifying colony forming units (CFUs). In the absence of treatment, 1928 colonies were formed on the agar plate. However, upon treatment with c-AgNPs, the plate yielded 984 colonies. Notably, negligible numbers of colonies (18 and 4), were developed on plates treated with b-Cs-AgNPs (30 μM) and b-Cs-AgNPs (50 μM), respectively. A plate treated with ampicillin (30 μM) exhibited 42 colonies. Comparing the experimental groups, a marked decrease in colony count was evident specifically within the b-Cs-AgNPs (30 μM) and b-Cs-AgNPs (50 μM) groups (Supporting Fig. 6a). This reduction underscores the potent antibacterial effect of b-Cs-AgNPs, surpassing the impact of other tested groups (Fig. 5b–f).

Agar disc diffusion method confirmed anti-bacterial effects of b-Cs-AgNPs

We conducted an agar disc diffusion method to check the antibacterial activity of b-Cs-AgNPs against different bacterial strains (*E. coli and B. subtills*). The diameters of clear zones around the wells were measured individually. The findings from the antimicrobial analysis distinctly demonstrated the susceptibility of the bacteria to both b-Cs-AgNPs and c-AgNPs. Notably, the zone of inhibition for bacteria treated with ampicillin was 24.54 mm. Meanwhile, b-Cs-AgNPs (30 μM) and c-AgNPs (30 μM) exhibited identical inhibition zones of 16.36 mm. b-Cs-AgNPs (50 μM) displayed a maximum zone of inhibition measuring 19.09 mm in *E. coli* whereas, it shows a zone of inhibition of 12.34 mm in *B. subtilis* (Fig. 5g, h). The results show that b-Cs-AgNPs are less toxic in nonpathogenic *B. subtills* bacteria in comparison to *E. coli* that can be simultaneously commensal or pathogenic depending physiological conditions [50]. These results clearly demonstrate the potent anti-bacterial efficacy of b-Cs-AgNPs in dose-dependent manner and can be utilized for the treatment of various infection models and mitigating biofilm formation on medical catheters. Furthermore, the influence of shape, size and surface charge of b-Cs-AgNPs in their antibacterial (Supporting Fig. 6c) and antibiofilm properties (Supporting Fig. 6b) are studied using zone of inhibition and *CV* staining assay.

In ovo infection model in chicken egg showed anti-infection properties of b-Cs-AgNPs

To demonstrate the efficiency of b-Cs-AgNPs preventing bacterial infection towards in vivo chicken egg models, various alginate discs containing the biosynthesized and chemically synthesized silver nanoparticles (Supporting Fig. 6d) were introduced into a 4-day-old *E. coli*-infected

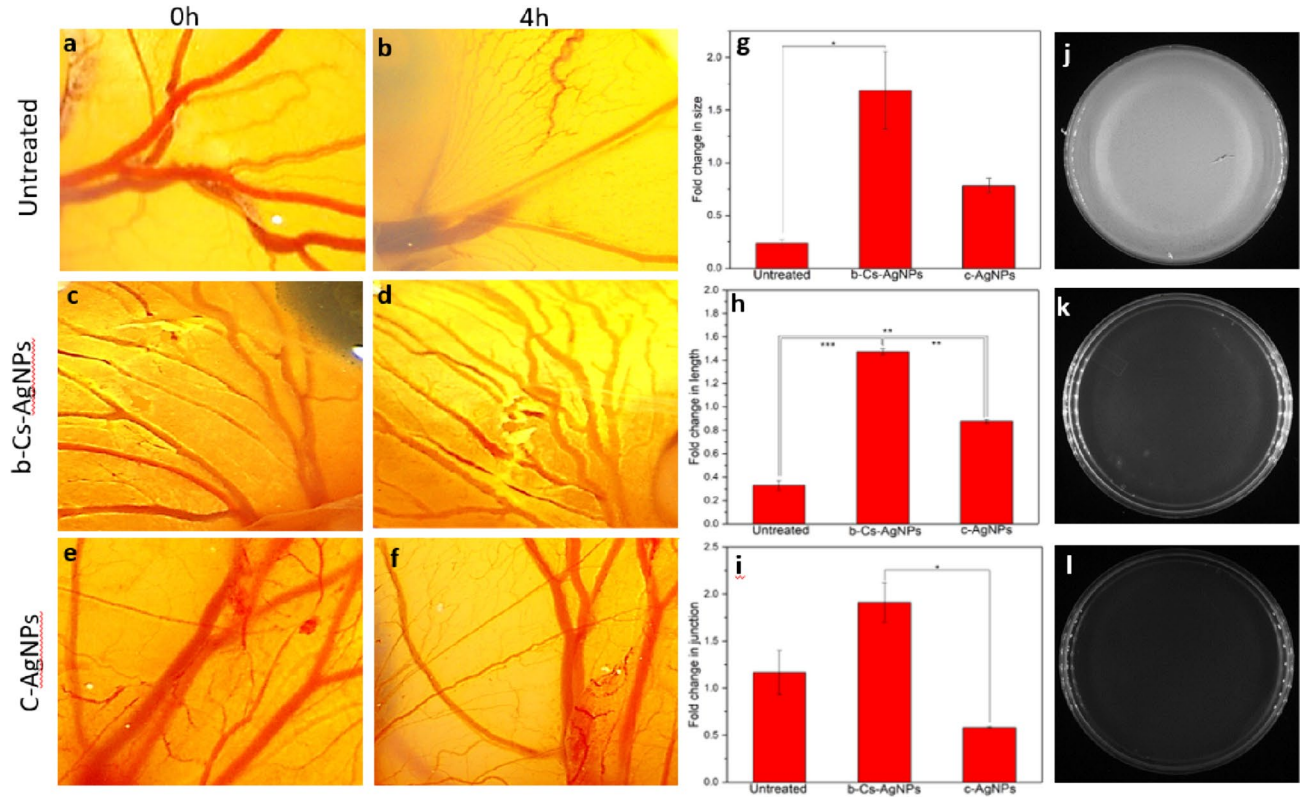

Fig. 6 CAM assay **a**–**f** shows the microscopic images of untreated, b-Cs-AgNPs, and c-AgNPs treated infectious chick embryo models at 0 h and 6 h. **g**–**i** The images are quantified with respect to length, junction, and size using ImageJ and Angiotool software. Significant differences of fold change in size, length and junction were observed between untreated, b-Cs-AgNPs and c-AgNPs treated samples (*$p < 0.05$, **$p < 0.005$, ***$p < 0.0005$), **j**–**l** colony forming assay employed by allantoic fluid of untreated, b-Cs-AgNPs and c-AgNPs

chick embryo. Following a 4-h treatment period, images were captured for comparison with the initial conditions at 0 h (as depicted in Fig. 6a–f). It was observed that the untreated samples exhibited a reduction in both the size and length of blood vessels, accompanied by an increase in the number of junctions after the 4-h treatment period. Comparatively, the b-Cs-AgNPs exhibited a more pronounced effect, leading to a greater fold change in the size, length, and junctions of blood vessels when compared to both c-AgNPs and the untreated samples (as illustrated in Fig. 6g–i).

Furthermore, we conducted agar plate experiments by incubating them with allantoic fluid collected from untreated embryos. These plates displayed a dense bacterial growth, forming a mat-like structure (as seen in Fig. 6j). However, when allantoic fluid from c-AgNP-treated embryos was used, fewer colonies were observed (as shown in Fig. 6k). Remarkably, almost no colonies were formed on plates treated with allantoic fluid from b-Cs-AgNP-treated embryos (as depicted in Fig. 6l). This indicates the superior antibacterial efficacy of b-Cs-AgNPs in inhibiting bacterial growth compared to both untreated and c-AgNP-treated samples.

b-Cs-AgNPs showed potent anti-biofilm properties

CV staining confirmed lower bacterial adhesion to medical catheters coated with b-Cs-AgNPs

Pathogenic bacteria often adopt a biofilm growth pattern as a defense mechanism against antimicrobial substances [51]. The most effective strategy to address infections rooted in biofilms involves obstructing their formation. In this assay, *crystal violet* (CV) dye is utilized to stain the extracellular polymeric substance (EPS) generated within the biofilm of the coated and uncoated catheters (Fig. 7a, b). This staining offers indirect confirmation of the presence of biofilm biomass [52]. The biofilms stained with *CV* indicated substantial surface coverage in the untreated control group. Notably, both b-Cs-AgNPs and c-AgNPs treatments significantly hindered biofilm development. When comparing these three groups, it was observed that b-Cs-AgNPs exhibited the most significant reduction in biofilm growth (67%) whereas c-AgNPs showed 45% biofilm inhibition rate (Fig. 7c).

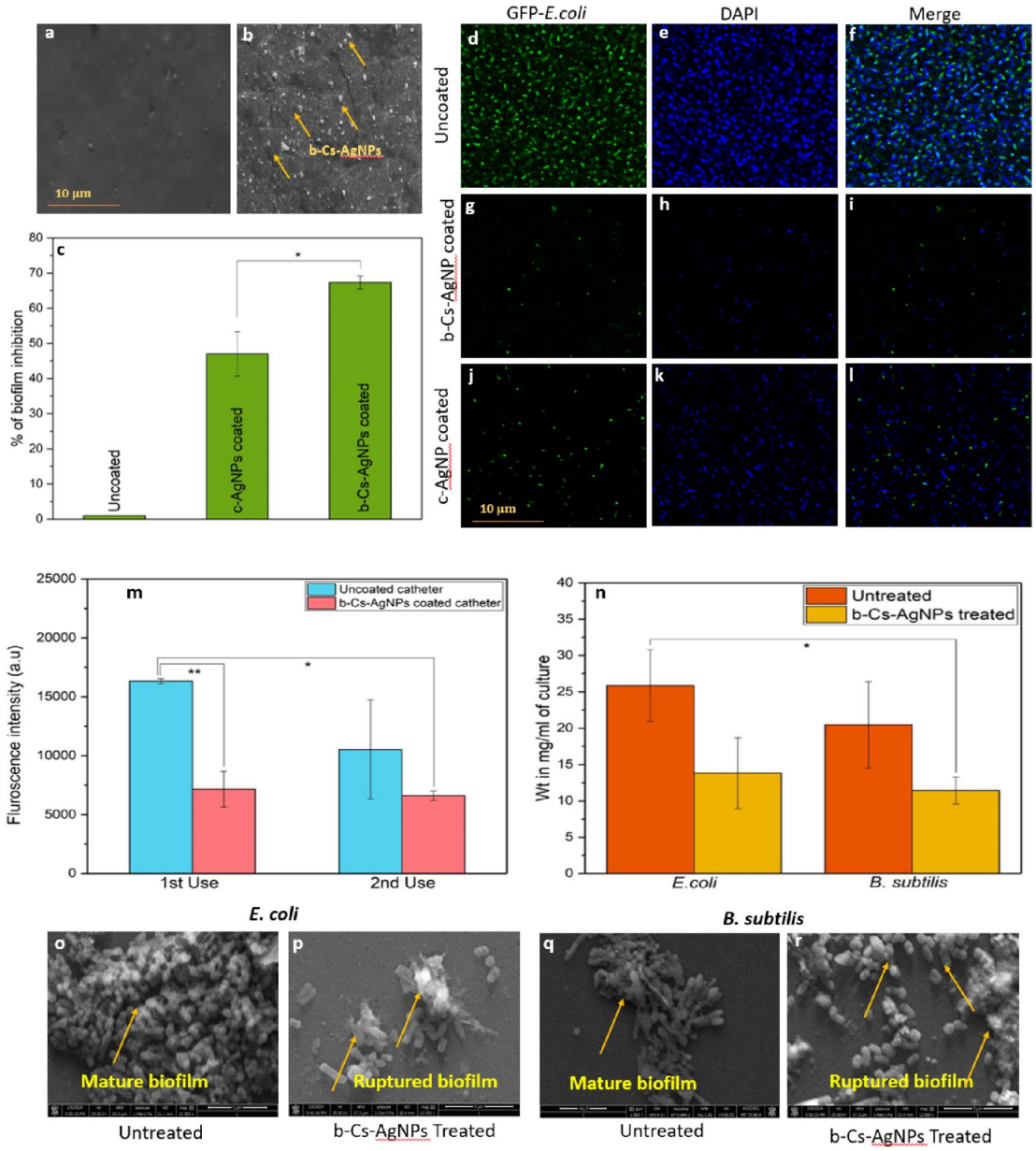

Fig. 7 SEM images of **a** uncoated and **b** b-Cs-AgNPs coated catheter, **c** CV staining assay indicating effects of b-Cs-AgNPs and c-AgNPs in preventing biofilm growth. Significant differences in absorbance was observed between untreated, b-Cs-AgNPs and c-AgNPs treated samples (*$p < 0.05$, ** $p < 0.005$), **d–l** confocal microscopy images of biofilm on uncoated and coated b-Cs-AgNPs and c-AgNPs catheters, **m** Fluorescence intensity of b-Cs-AgNPs coated catheter after subsequent uses confirmed antibiofilm abilities of b-Cs-AgNPs coating over prolonged use. **n** EPS obtained from bacterial suspension incubated with and without b-Cs-AgNPs, **o–r** SEM images showing effects of b-Cs-AgNPs in biofilm formation

Confocal microscopy established minimal bacterial viability in catheters coated with b-Cs-AgNPs

Utilizing confocal laser scanning microscopy (CLSM), we visually verified the impact of AgNPs on eliminating biofilms. In the images (Fig. 7d–l), it became evident that the untreated group exhibited a higher count of cells compared to both the b-Cs-AgNPs and c-AgNPs treated groups (Fig. 7d, g, j). To assess the overall population of live and deceased bacteria in the samples, *DAPI* staining was employed. It is evident that a larger number of bacteria adhered to the untreated samples, while significantly fewer attachments were observed in the b-Cs-AgNPs group. Furthermore, it was observed that the morphology of the bacteria displayed distinctive changes. In both the untreated and c-AgNPs-treated samples, the bacteria exhibited an

elongated form. However, in the case of the b-Cs-AgNPs-treated sample, a transformation was observed as the bacteria assumed an oval shape. This alteration strongly suggests that the b-Cs-AgNPs treatment had a detrimental effect on the structural integrity of the bacteria, causing a shift in their typical shape.

Reusability study indicated sustained antibiofilm activity over multiple uses

The fluorescence intensity of the bacterial suspension significantly decreased when incubated with b-Cs-AgNPs-coated catheters compared to uncoated catheters after the first use. Remarkably, even after the second use, the fluorescence intensity remained lower for the b-Cs-AgNPs-coated catheters, indicating sustained antibiofilm activity over multiple uses. This finding implies that even after extended use, the b-Cs-AgNPs coating continues to effectively inhibit biofilm formation (Fig. 7m).

SEM analysis revealed b-Cs-AgNPs ruptures mature biofilm of both *B. subtilis* and *E. coli*

The ability of b-Cs-AgNPs to disrupt mature biofilms formed by various bacterial strains (*E. coli* and *B. subtilis*), and their impact on biofilm architecture and integrity was evaluated using SEM analysis. The SEM images revealed that the biofilm treated with b-Cs-AgNPs lost its structural integrity and architecture (Fig. 7p, r). In contrast, the untreated bacteria (*E. coli* and *B. subtilis*) maintained its structure and developed a mature biofilm (Fig. 7o, q). This finding suggests that b-Cs-AgNPs damages the bacterial wall and structural proteins damaging the integrity of the mature biofilm.

Antibacterial activity of ferulic acid (FA): possible phytoconstituent present in leaf extract of Cs responsible for enhanced anti-bacterial activity of silver nanoparticles

The role of FA in reduction of $AgNO_3$ was initially confirmed by the change in color of the reaction from transparent to pale yellow. Further, we checked the absorbance of the solution and found that it showed maximum absorbance at 340 nm, which suggests that the OH group present in FA played a vital role in reducing $AgNO_3$-forming AgNPs (Supporting Fig. 7a) [53]. Moreover, DLS analysis revealed the size of NPs formed has an average size of 562.66 nm. It has been previously documented that Cs leaves contain Ferulic Acid (FA), which possesses antibacterial properties [26, 54]. This suggests that in the case of b-Cs-AgNPs, combining the antibacterial attributes of silver (Ag) with the presence of FA in Cs leaves enhances the bactericidal efficiency of b-Cs-AgNPs. To evaluate the antibacterial impact of FA, we exposed bacteria to FA at two distinct concentrations (0.5 mg/mL and 1 mg/mL) and observed that as the FA concentration increased, its bactericidal effectiveness also escalated (Supporting Fig. 7b).

Possible mechanistic analysis for anti-bacterial and anti-biofilm properties of b-Cs-AgNPs using molecular docking analysis

Docking analysis is a valuable resource for researchers in deciphering the precise molecular mechanisms underlying protein–ligand interactions. When experimental data is inaccessible in certain instances, docking strategies offer a pathway to comprehending cellular processes' molecular intricacies [55]. In our research, we employed this methodology to investigate the biological interactions between the active components of plant extract (ferulic acid) and molecular targets situated within bacteria for their survival and bacterial biofilm production (Supporting Information, Scheme 1). The aqueous extract of Cs leaves has been found to contain ferulic acid (FA), which aids in the reduction of silver and the formation of silver nanoparticles due to the presence of phenolic OH. In addition, it possesses antibacterial and antibiofilm properties [56]. It has been reported that FA cause pore formation in bacterial membrane causing leakage of intracellular matters [56]. We hypothesized that FA would cause enhanced antibacterial effects as it will be conjugated from the Cs extract to the synthesized b-Cs-AgNPs. Due to its important role in both synthesis and antibacterial activity, FA was chosen. According to research, PgaB and DosC aid in the formation of biofilms that protect bacteria from antibiotics and unfavorable environmental conditions, whereas GyraseB and FabH are necessary for *E. coli* growth and multiplication [57–59]. Targets are chosen based on the essential proteins of *E. coli* that are vital to the bacterium's survival. The target's binding affinity for FA demonstrated its important role in killing *E. coli* by inhibiting or blocking these vital proteins.

Gyrase B (pdb 1KZN) oversees DNA's ATP-dependent negative supercoiling (Fig. 8b, f). The replication in bacteria would be significantly impacted if the ATPase of gyrase B was inhibited [60]. Fatty acid biosynthesis (FAB) is a fundamental metabolic pathway for prokaryotic organisms, and it is indispensable for their cell survival and growth. FabH (Fig. 8a, e) emerges as a highly promising target in the quest for designing innovative antimicrobial drugs. This is primarily because FabH plays a pivotal role in modulating the pace of fatty acid biosynthesis through an initiation pathway. Moreover, its selectivity for specific substrates is a crucial determinant in shaping the composition of membrane fatty acids. Consequently, inhibiting FabH can disrupt this vital process, making it an efficient target for the development of

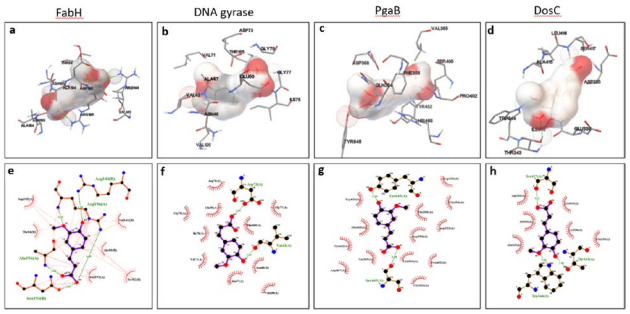

Fig. 8 **a**–**h** The graphical illustration of docked protein and Ferulic acid with their hydrogen bonding and interacting residues in 3D and 2D format **c, g** FabH **d, h** DNA gyrase

novel antimicrobial compounds [61]. In *E. coli*, the adhesion protein pgaB (Fig. 8c, g) plays a vital role in biofilm formation and structural stability. DosC (Fig. 8d, h) controls and influences biofilm formation in an oxygen-dependent manner [62].

Eventually, pgaB, which belongs to the same gene family, also affects biofilm formation. The docking results are presented in terms of the lowest energy of binding (LEB) for each compound. A lower LEB value indicates a stronger binding affinity between the compound and the target. Additionally, we examined hydrogen bonds, which are among the most robust interactions, as well as hydrophobic bonds, including carbon–hydrogen bonds, van der Waals forces, Pi-sigma interactions, Pi-Pi interactions, and others. The LEB value for FabH, DNA gyrase, PgaB and DosC are −9.68 kcal/mol, −8.07 kcal/mol, −9.19 kcal/mol and −8.20 kcal/mol, respectively. Each docked structure contains 5, 2, 1 and 3 hydrogen bonds, respectively (Table 3). The Results show that ferulic acid has an excellent binding affinity towards the essential survival protein and the biofilm-associated proteins of *E. coli*, and the probable crucial phytoconstituent present in the Cs leaf causing anti-bacterial and anti-biofilm properties of b-Cs-AgNPs along with well-established silver NPs.

Overall discussion

In this research, we have introduced a sustainable, cost-effective, and eco-friendly approach to synthesize b-Cs-AgNPs. The intent behind using green synthesis method is to minimize the use of harmful chemicals and energy-intensive processes. Our findings highlighted, b-Cs-AgNPs antibiofilm coatings as a promising advancement in fighting healthcare-assisted infections, more specifically catheter-associated infections. Upon comparison with other NPs used for similar coating purposes, several significant differences were observed preventing biofilm formation. Firstly, CAM and MTT assay clearly demonstrated that b-Cs-AgNPs are better compatible with biological systems compared to c-AgNPs. Additionally, even after prolonged exposure to b-Cs-AgNPs, the rat skin does not exhibit any signs of inflammation. Moreover b-Cs-AgNPs shows well tolerance in *E. coli* infected chick embryo model, in contrast to certain other metal nanoparticles like copper or zinc, which can have cytotoxic effects on host cells [63]. Such biocompatibility is essential for medical applications, where patient safety is the primary concern.

Our synthesized b-Cs-AgNPs exhibited comparable or better anti-bacterial and anti-biofilm efficacy in contrast to existing NPs. We have replicated the synthesis of nanoparticles under similar reaction conditions, and each time, we have observed that the resulting NPs are spherical in shape and fall in the 80–120 nm size range as indicated by the DLS results. The reproducibility of the product was also analyzed for its antibacterial property and found that it shows similar effects every time it is synthesized. The findings demonstrate that the process of synthesizing NPs is reliable and repeatable and exhibits consistent antibacterial and antibiofilm properties in different batches of synthesis.

Table 3 Molecular docking analysis of ferulic acid with *E. coli* proteins

Serial no	Macromolecule name	PDB ID	RMSD	Free binding energy (kcal/mol)	Inhibitory constant	H bond	Interacting residues
1	Beta-ketoacyl-[acyl carrier protein] synthase iii (FabH)	1EBL	58.042	−9.68	80.48 nM	5	ALA194 ASN193 ARG144 ARG196
2	DNA gyrase subunit b	1KZN	51.669	−8.07	1.21 µM	2	GLY77 VAL43
3	*Escherichia coli* PgaB C-terminal domain	4P7O	58.059	−9.19	182.18 nM	1	TYR645
4	Diguanylate cyclase DosC	4ZVF	25.076	−8.20	979.57 nM	3	THR343 TRP344 SER417

It has been reported that zinc oxide NPs typically shows a spherical shape, with size falling within the range of 30–63 nm showing a zone of inhibition (ZOI) of approximately 9 mm [64]. In comparison, b-Cs-AgNPs maintains a spherical shape and the average size falls between the range of 9–10 nm. The highest ZOI obtained for cadmium sulfide (CdS) NPs against *E. coli* achieved at a concentration of 80 µg/mL was found to be 11.5 mm [65]. On the other hand, at a lower concentration of 30 µM, b-Cs-AgNPs displayed a larger zone of 16.36 mm against *E. coli* and 10.32 mm against *B. subtilis*. Additionally, b-Cs-AgNPs also protected *E. coli* infected chick embryo model at a very lower concentration of 8 µM within a small duration of 4 h. The average size of AgNPs synthesized utilizing *Tectona grandis* seeds extract lies between 10 and 30 nm, displaying ZOI of 17 mm at a concentration of 50 µg [66]. In contrast, zones measuring 6 to 10 mm were observed at different concentration of AgNPs produced from the aqueous rhizome extract of *Coptis chinensis* [67]. According to these reports, we can conclude that our b-Cs-AgNPs are superior to zinc oxide NPs, CdS NPs, and AgNPs obtained from different sources in many ways. b-Cs-AgNPs exhibited several advantages which include a smaller average size, spherical morphology, and significantly enhanced antibacterial activity, as indicated by the larger ZOI observed at a lower concentration. Additionally, b-Cs-AgNPs demonstrated strong antioxidant properties and better biocompatibility useful for many applications.

Unlike previous studies that primarily focuses on in vitro experiments to demonstrate antibacterial properties of a sample, we conducted both in vivo and in vitro studies to identify antibacterial and anti-infection abilities of b-Cs-AgNPs [54, 55]. 4-day-old *E. coli*-infected chick embryo model was used to perform in vivo study and found that b-Cs-AgNPs can suppress bacterial growth within a short period of 4 h. It was also observed that b-Cs-AgNPs are non-toxic causing no harm to the developing embryo and do not interfere with the process of angiogenesis. Furthermore, the coating process of medical catheter is very simple, requiring only a single step and taking just 12 h, as opposed to other methods that are complex and more time consuming [56, 68]. Moreover, unlike other nanoparticles b-Cs-AgNPs not only prevent bacterial attachment over catheter surfaces but also alter the morphology of attached bacteria. b-Cs-AgNPs reduce the possibilities of bacterial colonization on the catheter's surface by inhibiting their initial attachment. Altered morphology and inability of biofilm formation makes the bacteria more vulnerable to antimicrobial treatments and less resistant to host's immune cells [58, 59]. This increases the effectiveness of b-Cs-AgNPs over other coating materials. Many researchers fail to explain the mechanism behind antibacterial and antibiofilm properties of their sample [59]. In our study, we performed molecular docking to understand possible mechanism beneath antibacterial and antibiofilm behaviour of b-Cs-AgNPs. The processes employed by b-Cs-AgNPs in combating bacterial infection and biofilm generation can be well understood using molecular docking. Results of docking analysis revealed that ferulic acid present within b-Cs-AgNPs exhibits a strong binding affinity with specific bacterial proteins crucial for bacterial survival and biofilm formation.

We have performed all the anti-bacterial and toxicity studies for a maximum of 2 days. While b-Cs-AgNPs show good short-term biocompatibility, further studies may be required to investigate their long-term efficacy and safety when employed within the body. Additionally, the synthesis of b-Cs-AgNPs can have influence by environmental and seasonal conditions that needs through investigations. In addition, extensive tests will be conducted as part of our research to assess the effectiveness of b-Cs-AgNPs in healing a variety of wound types, including infective wounds. We will further investigate the potential application of b-Cs-AgNPs in water treatment systems, aiming to ensure the provision of safe and clean drinking water. Interdisciplinary collaboration is necessary to discover full potential of b-Cs-AgNPs providing innovative solutions to serious medical and environmental challenges.

Conclusion

Our research has presented a promising solution in response to the formidable challenge of combating biofilm-related infections, particularly catheter-associated urinary tract infections (CAUTIs). Biofilm-related infections are major concern for patient safety and healthcare practices accounting for approximately 80% of medical infections. Synthesized b-Cs-AgNPs were thoroughly examined using several characterization processes, confirming the successful synthesis of b-Cs-AgNPs, validating their suitability for further studies. Various in vitro and in vivo experiments were conducted to test the efficacy of these b-Cs-AgNPs as antimicrobial and antibiofilm agents. The results demonstrated that b-Cs-AgNPs offers a potential solution to the challenges posed by biofilm-related infections on medical device by combating bacterial infections and inhibiting biofilm formation.

Supplementary Information The online version contains supplementary material available at https://doi.org/10.1007/s00775-024-02050-4.

Acknowledgements LP and AU thank UGC, New Delhi for their junior research fellowship. Dr Sudip Mukherjee acknowledges director (Prof. Pramod Kumar Jain), Indian Institute of Technology (BHU) for providing research infrastructure and other facilities. SM further acknowledged research fund support from IIT (BHU) [OH-35-Other Capital/Miscellaneous Grant] and the Royal Society of Chemistry, UK (No. R22-2922732087) for providing funding support for this work. Authors acknowledges Vaishali Yadav and Dr. Bama Charan Mondal,

Department of Zoology, Banaras Hindu University, Varanasi, UP, India for helping in the confocal microscopic analysis and generously providing GFP-*E. coli*, respectively.

Author contributions LP and SM has conceptualized the idea of this manuscript. LP, PS, MN, GS, AI, PP have performed the experiments, developed the methodology, and validated the results. SM and LP has written the original draft of the manuscript and revised. SM has acquired the funding and supervised the overall work as the corresponding author.

Funding IIT (BHU) [OH-35-Other Capital/Miscellaneous Grant] and the Royal Society of Chemistry, UK (No. R22-2922732087).

Data availability All data related to the manuscript will be readily available upon request.

Declarations

Conflict of interest The authors declare that they have no known competing financial interests or personal relationships that could have appeared to influence the work reported in this paper.

Ethical approval Dermal skin irritation study was performed after IAEC approval (IIT(BHU)/IAEC/2023/068; Approval Date: February 9, 2023).

Declaration of generative AI in scientific writing No AI support was taken during the preparation of the manuscript at any stage.

References

1. Bhardwaj T, Ramana LN, Sharma TK (2022) Current advancements and future road map to develop ASSURED microfluidic biosensors for infectious and non-infectious diseases. Biosensors 12(5):357
2. Arney D, Venkatasubramanian KK, Sokolsky O, Lee I (2011) Biomedical devices and systems security. In: 2011 Annual international conference of the IEEE engineering in medicine and biology society, 2011, pp. 2376–2379
3. Magill SS et al (2014) Multistate point-prevalence survey of health care-associated infections (in eng). N Engl J Med 370(13):1198–1208
4. Noimark S, Dunnill CW, Wilson M, Parkin IP (2009) The role of surfaces in catheter-associated infections (in eng). Chem Soc Rev 38(12):3435–3448
5. Burroughs L, Ashraf W, Singh S, Martinez-Pomares L, Bayston R, Hook AL (2020) Development of dual anti-biofilm and anti-bacterial medical devices (in eng). Biomater Sci 8(14):3926–3934
6. Keum H et al (2017) Prevention of bacterial colonization on catheters by a one-step coating process involving an antibiofouling polymer in water. ACS Appl Mater Interfaces 9(23):19736–19745
7. Francolini I, Donelli G, Stoodley P (2003) Polymer designs to control biofilm growth on medical devices. Rev Environ Sci Biotechnol 2(2):307–319
8. Gwisai T et al (2017) Repurposing niclosamide as a versatile antimicrobial surface coating against device-associated, hospital-acquired bacterial infections (in eng). Biomed Mater 12(4):045010
9. Cloutier M, Mantovani D, Rosei F (2015) Antibacterial coatings: challenges, perspectives, and opportunities. Trends Biotechnol 33(11):637–652
10. Ding X et al (2012) Antibacterial and antifouling catheter coatings using surface grafted PEG-b-cationic polycarbonate diblock copolymers. Biomaterials 33(28):6593–6603
11. Woo J et al (2020) Facile synthesis and coating of aqueous antifouling polymers for inhibiting pathogenic bacterial adhesion on medical devices. Prog Org Coat 147:105772
12. Sohns JM, Bavendiek U, Ross TL, Bengel FM (2017) Targeting cardiovascular implant infection: multimodality and molecular imaging (in eng). Circ Cardiovasc Imaging 10(12)
13. Devine R, Singha P, Handa H (2019) Versatile biomimetic medical device surface: hydrophobin coated, nitric oxide-releasing polymer for antimicrobial and hemocompatible applications. Biomater Sci 7(8):3438–3449. https://doi.org/10.1039/C9BM00469F
14. Damodaran VB, Murthy NS (2016) Bio-inspired strategies for designing antifouling biomaterials (in eng). Biomater Res 20:18
15. Zheng W, Jia Y, Chen W, Wang G, Guo X, Jiang X (2017) Universal coating from electrostatic self-assembly to prevent multidrug-resistant bacterial colonization on medical devices and solid surfaces (in eng). ACS Appl Mater Interfaces 9(25):21181–21189
16. Martinez-Gutierrez F et al (2013) Anti-biofilm activity of silver nanoparticles against different microorganisms. Biofouling 29(6):651–660
17. Loo C-Y, Young PM, Lee W-H, Cavaliere R, Whitchurch CB, Rohanizadeh R (2014) Non-cytotoxic silver nanoparticle-polyvinyl alcohol hydrogels with anti-biofilm activity: designed as coatings for endotracheal tube materials. Biofouling 30(7):773–788
18. Ashmore DA et al (2018) Evaluation of *E. coli* inhibition by plain and polymer-coated silver nanoparticles. Revista do Instituto de Medicina Tropical de São Paulo 60:e18.
19. Sahoo B et al (2023) Photocatalytic activity of biosynthesized silver nanoparticle fosters oxidative stress at nanoparticle interface resulting in antimicrobial and cytotoxic activities. Environ Toxicol
20. Campo-Beleño C et al (2022) Biologically synthesized silver nanoparticles as potent antibacterial effective against multidrug-resistant *Pseudomonas aeruginosa*. Lett Appl Microbiol 75(3):680–688
21. Mukherjee S et al (2014) Potential theranostics application of bio-synthesized silver nanoparticles (4-in-1 system). Theranostics 4(3):316
22. Rajan R, Chandran K, Harper SL, Yun S-I, Kalaichelvan PT (2015) Plant extract synthesized silver nanoparticles: an ongoing source of novel biocompatible materials. Indust Crops Prod 70:356–373
23. Omar SM, Ahmat N, Nik Azmin NF, Sabandar CW, Muqarrabun A, Ramadhan LM (2013) Isolation and characterization of chemical constituents from the flower of *Calliandra surinamensis* benth. Open Conf Proc J 4(1)
24. Falodun A, Irabor EE (2008) Phytochemical, proximate, antioxidant and free radical scavenging evaluations of *Calliandria surinamensis* (in eng). Acta Pol Pharm 65(5):571–575
25. Procópio TF et al (2017) CasuL: a new lectin isolated from *Calliandra surinamensis* leaf pinnulae with cytotoxicity to cancer cells, antimicrobial activity and antibiofilm effect. Int J Biol Macromol 98:419–429
26. Alzahrani A, Abbott G, Young L, Igoli J, Gray A, Ferro V (2016) Phytochemical and biological investigation of *Calliandra surinamensis* as a potential treatment for diabetes. Planta Med 82(Suppl. 01):P385
27. Somba GC, Edi HJ, Siampa JP (2019) Formulasi sediaan krim ekstrak etanol daun kaliandra (*Calliandra surinamensis*) dan uji aktivitas antibakterinya terhadap bakteri *Staphylococcus aureus*. Pharmacon 8(4):809–814
28. Domitrović R, Rashed K, Cvijanović O, Vladimir-Knežević S, Škoda M, Višnić A (2015) Myricitrin exhibits antioxidant, anti-inflammatory and antifibrotic activity in carbon

tetrachloride-intoxicated mice (in eng). Chem Biol Interact 230:21–29
29. Saleem M (2009) Lupeol, a novel anti-inflammatory and anti-cancer dietary triterpene. Cancer Lett 285(2):109–115
30. Pirtarighat S, Ghannadnia M, Baghshahi S (2019) Green synthesis of silver nanoparticles using the plant extract of *Salvia spinosa* grown in vitro and their antibacterial activity assessment. J Nanostruct Chem 9(1):1–9
31. Patra S, Mukherjee S, Barui AK, Ganguly A, Sreedhar B, Patra CR (2015) Green synthesis, characterization of gold and silver nanoparticles and their potential application for cancer therapeutics. Mater Sci Eng C 53:298–309
32. Xiao F, Xu T, Lu B, Liu R (2020) Guidelines for antioxidant assays for food components. Food Front 1(1):60–69
33. Chowdhury SR, Mukherjee S, Das S, Patra CR, Iyer PK (2017) Multifunctional (3-in-1) cancer theranostics applications of hydroxyquinoline-appended polyfluorene nanoparticles. Chem Sci 8(11):7566–7575. https://doi.org/10.1039/C7SC03321D
34. Keshari AK, Srivastava R, Singh P, Yadav VB, Nath G (2020) Antioxidant and antibacterial activity of silver nanoparticles synthesized by *Cestrum nocturnum*. J Ayurveda Integr Med 11(1):37–44
35. García-Gareta E, Binkowska J, Kohli N, Sharma V (2020) Towards the development of a novel ex ovo model of infection to pre-screen biomaterials intended for treating chronic wounds. J Funct Biomater 11(2):37
36. Mukherjee S et al (2023) Screening hydrogels for antifibrotic properties by implanting cellularly barcoded alginates in mice and a non-human primate. Nat Biomed Eng 7(7):867–886
37. Kragh KN, Alhede M, Kvich L, Bjarnsholt T (2019) Into the well—a close look at the complex structures of a microtiter biofilm and the crystal violet assay. Biofilm 1:100006
38. Siddique MH et al. (2020) Effect of silver nanoparticles on biofilm formation and EPS production of multidrug-resistant *Klebsiella pneumoniae.* BioMed Res Int 6398165
39. Laskowski RA, Swindells MB (2011) LigPlot+: multiple ligand–protein interaction diagrams for drug discover. ACS Publications
40. Kerker M (1985) The optics of colloidal silver: something old and something new. J Colloid Interface Sci 105(2):297–314
41. Magdassi S, Bassa A, Vinetsky Y, Kamyshny A (2003) Silver nanoparticles as pigments for water-based ink-jet inks. Chem Mater 15(11):2208–2217
42. Kotcherlakota R et al (2019) Biosynthesized gold nanoparticles: in vivo study of near-infrared fluorescence (NIR)-based bioimaging and cell labeling applications. ACS Biomater Sci Eng 5(10):5439–5452
43. Allaka G, King MFL, Yepuri V, Narayana RL (2023) Synthesis of silver oxide nanoparticles using gomutra mediation and their investigations on anti-oxidant property. Mater Today: Proc
44. Korkmaz N, Karadağ A (2021) Microwave assisted green synthesis of Ag, Ag_2O, and Ag_2O_3 nanoparticles. J Turkish Chem Soc Sect A: Chem 8(2):585–592
45. He Y et al (2017) Green synthesis of silver nanoparticles using seed extract of Alpinia katsumadai, and their antioxidant, cytotoxicity, and antibacterial activities. RSC Adv 7(63):39842–39851. https://doi.org/10.1039/C7RA05286C
46. Mochalin V, Osswald S, Gogotsi Y (2009) Contribution of functional groups to the Raman spectrum of nanodiamond powders. Chem Mater 21(2):273–279
47. Allafchian AR, Mirahmadi-Zare SZ, Jalali SAH, Hashemi SS, Vahabi MR (2016) Green synthesis of silver nanoparticles using phlomis leaf extract and investigation of their antibacterial activity. J Nanostruct Chem 6(2):129–135
48. Konappa N et al (2021) Ameliorated antibacterial and antioxidant properties by *Trichoderma harzianum* mediated green synthesis of silver nanoparticles. Biomolecules 11(4):535
49. Bassetti S, Tschudin-Sutter S, Egli A, Osthoff M (2022) Optimizing antibiotic therapies to reduce the risk of bacterial resistance. Eur J Intern Med 99:7–12
50. Ahmad SA et al (2020) Bactericidal activity of silver nanoparticles: a mechanistic review. Mater Sci Energy Technol 3:756–769
51. Singh S, Singh SK, Chowdhury I, Singh R (2017) Understanding the mechanism of bacterial biofilms resistance to antimicrobial agents (in eng). Open Microbiol J 11:53–62
52. Bala Subramaniyan S, Senthilnathan R, Arunachalam J, Anbazhagan V (2020) Revealing the significance of the glycan binding property of Butea monosperma seed lectin for enhancing the antibiofilm activity of silver nanoparticles against uropathogenic *Escherichia coli*. Bioconjugate Chem 31(1):139–148
53. Mikhlif H (2019) Ecofriendly route for waste upcycling and silver nanoparticles synthesis from citrus reticulata Peel. Int J Nanoelectron Mater 12:349–356
54. Procópio TF et al (2018) *Calliandra surinamensis* lectin (CasuL) does not impair the functionality of mice splenocytes, promoting cell signaling and cytokine production. Biomed Pharmacother 107:650–655
55. McConkey BJ, Sobolev V, Edelman M (2022) The performance of current methods in ligand–protein docking. Curr Sci 845–856
56. Borges A, Ferreira C, Saavedra MJ, Simões M (2013) Antibacterial activity and mode of action of ferulic and gallic acids against pathogenic bacteria. Microb Drug Resist 19(4):256–265
57. Gross CH et al (2003) Active-site residues of *Escherichia coli* DNA gyrase required in coupling ATP hydrolysis to DNA supercoiling and amino acid substitutions leading to novobiocin resistance (in eng). Antimicrob Agents Chemother 47(3):1037–1046
58. Whaley SG, Rock CO (2020) Alternate fatty acid synthesis initiation in *Escherichia coli*. FASEB J 34(S1):1–1
59. Scotti R, Casciaro B, Stringaro A, Maggi F, Colone M, Gabbianelli R (2024) Fighting microbial infections from *Escherichia coli* O157: H7: the combined use of three essential oils of the cymbopogon genus and a derivative of Esculentin-1a peptide. Antibiotics 13(1):86
60. Couturier M, Bahassi EM, Van Melderen L (1998) Bacterial death by DNA gyrase poisoning. Trends Microbiol 6(7):269–275
61. Lu X, Tang J, Zhang Z, Ding K (2015) Bacterial β-ketoacyl-acyl carrier protein synthase III (FabH) as a target for novel antibacterial agents design. Curr Med Chem 22(5):651–667
62. Wang X, Preston JF III, Romeo T (2004) The pgaABCD locus of *Escherichia coli* promotes the synthesis of a polysaccharide adhesin required for biofilm formation. J Bacteriol 186(9):2724–2734
63. Dhahi RM, Mikhlif HM (2019) Ecofriendly route for waste upcycling and silver nanoparticles synthesis from citrus reticulata Peel. Int J Nanoelectron Mater 12(3)
64. Meruvu H, Vangalapati M, Chippada SC, Bammidi SR (2011) Synthesis and characterization of zinc oxide nanoparticles and its antimicrobial activity against *Bacillus subtilis* and *Escherichia coli*. J Rasayan Chem 4(1):217–222
65. Shivashankarappa A, Sanjay KR (2020) *Escherichia coli*-based synthesis of cadmium sulfide nanoparticles, characterization, antimicrobial and cytotoxicity studies. Braz J Microbiol 51:939–948
66. Rautela A, Rani J (2019) Green synthesis of silver nanoparticles from *Tectona grandis* seeds extract: characterization and

mechanism of antimicrobial action on different microorganisms. J Anal Sci Technol 10(1):1–10
67. Ahmad A et al (2017) The effects of bacteria-nanoparticles interface on the antibacterial activity of green synthesized silver nanoparticles. Microb Pathog 102:133–142
68. Gross CH et al (2003) Active-site residues of *Escherichia coli* DNA gyrase required in coupling ATP hydrolysis to DNA supercoiling and amino acid substitutions leading to novobiocin resistance. Antimicrobial Agents Chemother 47(3):1037–1046

Authors and Affiliations

Lipi Pradhan[1] · Prince Sah[1] · Malay Nayak[1] · Anjali Upadhyay[1] · Pragya Pragya[1] · Shikha Tripathi[2] · Gurmeet Singh[1] · B. Mounika[1] · Pradip Paik[1] · Sudip Mukherjee[1]

✉ Sudip Mukherjee
sudip.bme@iitbhu.ac.in

[1] School of Biomedical Engineering, IIT (BHU), Varanasi, India

[2] Department of Physics, IIT (BHU), Uttar Pradesh, Varanasi, India